Detection of Periodic Forced Oscillations in Power Systems Using Multitaper Approach

Md. Arif Khan , *Member, IEEE*, and John W. Pierre , *Fellow, IEEE*

Abstract—An algorithm based on Thomson's multitaper spectral estimation and harmonic analysis techniques is proposed for the detection and frequency estimation of periodic forced oscillations in a power system. Unlike traditional periodogram-based techniques, the method does not rely on true ambient noise spectrum of the system, and can operate continuously in an online environment without requiring any system knowledge except synchrophasor measurements. It compares a test statistic derived from only measurements against a threshold, and the threshold is established from general expressions of the test statistic's distribution and the probability of false alarm. Performance of the detector is explicitly expressed using probability of detection expression, and evaluated using simulation studies. Results upon application of this algorithm to field measured synchrophasor data suggest usability of the technique for forced oscillation detection in practical monitoring of the power system.

Index Terms—Detection, forced oscillation, harmonic analysis, multitaper, phasor measurement unit (PMU), power system dynamics, synchrophasor measurements.

I. INTRODUCTION

BOTH forced and electromechanical oscillations occur in power system. The increasing availability of high fidelity Global Positioning System (GPS) synchronized Phasor Measurement Unit (PMU) data enables detailed study of these oscillations for improving power system reliability. Forced oscillations (FOs) have been found noticeably present in system-wide PMU measurements in the U.S. eastern interconnection (EI), the western North American power system (wNAPS), and the Nordic power systems [1]. The electromechanical oscillations are natural phenomena of power system which dictate how a group of generators exchange mechanical and electrical energy with another group. Unlike system's natural oscillations, FOs are response of the system when driven by rogue inputs [2]. There are numerous causes that generate FOs in power systems [3]. Some of them are steam-turbine regulator malfunction [4], cyclic load [5], incautious power system

stabilizer (PSS) design [6], stable limit cycles induced by upper limits on generator field-voltage [7], faulty control [8], [9], and possibly wind turbines [8], [10]. The frequencies of FOs can vary considerably, and if the frequency of an FO coincides with any of the dominant electromechanical modes in the system, it will tend to strengthen the oscillation which magnitude will be governed by the damping of the free response mode [11]. The inter-area electromechanical modes were shown especially vulnerable to resonance from FOs in [12].

In the PMU measurements, FOs typically manifest themselves as sinusoids often with harmonics [2]. Consequently, FOs tend to severely bias the synchrophasor measurements based power system identification techniques, such as modified extended Yule Walker (YW) and YW With Spectral Analysis algorithms, that operate by estimating poles and/or zeros of a linear system [13]–[15]. This is true even if the amplitudes of the FOs are very small [15]. The bias can be reduced significantly if the FOs that are present in the measurements can be detected and accounted before employing the identification techniques. For example, the algorithms proposed in [15] and [16] were shown to provide improved electromechanical mode estimation performance by reducing the bias due to the presence of FOs. Both of the algorithms rely heavily on a prior estimation of all FOs present in the measurements for their improved performance. As a result, they require detection of FOs in the measurements and estimation of their frequencies prior to estimating the dominant electromechanical modes.

Comparing magnitude-squared coherence estimated from two time-series signals to a preset threshold an FO detection technique was proposed in [17]. The technique suffers when the two chosen signals are linearly correlated regardless of the presence of FOs in the signals. To circumvent the requirement of two signals, the method was further extended in [18] that employs self-coherence estimated from a signal and its time-delayed signal. It requires a large time delay so that coherence between ambient noise in the two segments is small and selection of a proper measurement channel. When no FO is present and the system is operating under ambient conditions, the energy in PMU measurements remain relatively constant from one time window to the next. In such a case, onset of an FO adds significant energy to the data. By detecting such increase in signal energy in predefined frequency bands an RMS-energy filtering approach for detecting FOs was presented in [19] and practical implementation of the technique was described in [20]. Since the technique examines a range of frequencies it can be

useful for detecting stochastic FOs having time-varying frequency characteristics.

In a few recent works, Follum *et al.* proposed periodogram based FOs detection and their frequency estimation techniques in [2], [21], [22]. The techniques operate by comparing estimated periodogram from a block of measurements to a threshold derived from prior knowledge of ambient noise spectrum in synchrophasor measurements. The technique proposed in [2] uses the true ambient noise spectrum of the system for setting the detection threshold. The true ambient noise spectrum of a large and interconnected power system is typically unknown for near-real time power system monitoring applications. The ambient noise is the natural response of the system to random load variations that provide small excitations to the electromechanical dynamics of the system [23], and it is always present in the PMU measurements. Both parametric and nonparametric spectral estimation techniques can estimate the ambient noise spectrum from synchrophasor measurements where no significant transients or FOs are present. If there is any significant FO present, a separable estimation of the ambient noise spectrum can be achieved using two-stage least squares and overdetermined modified Yule-Walker algorithms based on autoregressive moving average plus sinusoid model [15], [16]. But these techniques require detection of FOs for their operations. So there is an obvious dilemma of which comes first; ambient noise spectrum estimation or FOs detection. Thus, a technique that is capable of detecting FOs from only synchrophasor measurements without any prior system knowledge is required for power system monitoring applications.

Detection of FOs is important in its own right as FOs are indicative of some malfunctioning in the system [2]. The periodogram based detector mentioned earlier performs well as it uses prior knowledge of the ambient noise spectrum. In power system, the ambient noise spectrum typically changes gradually over time or can change more abruptly if there is a sudden system configuration change. Consequently, the detection threshold must be updated depending on the current system conditions for better detection performance. In a recent work, Follum *et al.* used modified Daniel-Welch (mDW) periodogram [24] for estimating the ambient noise spectrum from synchrophasor measurements containing FOs. The mDW applies a median filter across the frequencies of estimated power spectral density (PSD) from a window of power system measurements [21], [24]. It requires a large window of measurements for a good estimate. Also the length of the median filter for a certain analysis window length affects the PSD estimate that further affects the detector performance.

This paper proposes a method of detecting FOs in power system that does not require any prior knowledge of the system and is capable of detecting FOs from only the synchrophasor measurements. The proposed method does not require any apriori information about the ambient noise spectrum, but incorporates it being unknown into the formulation of the method. The approach is based on the multitaper spectral estimation and harmonic analysis procedures introduced by Thomson in 1982 [25], and is generalized for detecting FOs in power system in an online environment. Performance of the detection technique are

provided via expressions of probability of detection (P_D) and probability of false alarm (P_{FA}).

Following section outlines a general signal model for synchrophasor measurements containing periodic FOs. Based on this signal model, an FOs detection algorithm based on Thomson's multitaper spectral estimation and harmonic analysis is presented in Section III. Section IV applies the detection algorithm to simulated and field measured PMU data and discusses the results. Finally, Section V draws conclusive remarks of the works presented in this paper.

II. SIGNAL MODEL

Consider a discrete-time PMU measurement modeled as

$$y(n) = \eta(n) + s(n), \ n = 0, 1, ..., N - 1, \quad (1)$$

where $\eta(n)$ is steady-state response of power system acting upon random load variations, i.e., the ambient noise in synchrophasor measurements [23]. Typically, $\eta(n)$ is modeled as a zero-mean stochastic process [14]. The term $s(n)$ in the signal model accounts for the presence of any FOs. As FOs typically manifest themselves as sinusoids [2], they can be modeled as

$$s(n) = \sum_{r=1}^{N_{FO}} A_r \cos\left(2\pi f_r n T_s + \phi_r\right) I_{[n_s(r), n_e(r)]}(n), \quad (2)$$

where A_r, f_r, and ϕ_r are respectively the amplitude, frequency (in Hz), and phase of rth FO, and N_{FO} is total number of FOs present in the measurement $y(n)$. $T_s = 1/f_s$ is sampling interval (in sec.) where f_s is the sampling rate in samples per sec. The indicator function (see [26]) $I_{[n_s(r), n_e(r)]}(n)$ captures the duration of the rth sinusoid in detection window $\{y(n) : n \in [0, N-1]\} = \mathbf{y}$ of length N, and is defined as

$$I_{[n_s(r), n_e(r)]}(n) = \begin{cases} 1, & \text{if } 0 \leq n_s(r) \leq n \leq n_e(r) \leq N - 1 \\ 0, & \text{otherwise}, \end{cases}$$
$$(3)$$

where $n_s(r)$ and $n_e(r)$ are starting and ending sample indexes of the rth FO in the detection window $\mathbf{y}$, respectively. If the indicator function is not of immediate interest, it is abbreviated as $I_r(n)$ in the subsequent discussions. With the signal model formulated in (1), the following section discusses the multitaper FO detection algorithm in detail.

III. DETECTION ALGORITHM

In this section, the development of the multitaper FO detection algorithm based on the signal model established in the previous section is discussed in detail. At first, a complex linear regression model is formed based on discrete Fourier transform (DFT) of the signal. Based on the regression model, the FO detection problem is formulated as a statistical hypothesis test. The test compares a test statistic (SubSection III-A) to a threshold (SubSection III-B), and the value of the test statistic is calculated from only the synchrophasor measurements and some user chosen tapers. In SubSection III-C two types of tapers that can be used for the detection algorithm are briefly discussed.

SubSection III-D briefly outlines extension of the detection algorithm for examining multiple detection segment. The frequencies of the detected FOs can be refined and SubSection III-E discusses the refinement methods. The implementation of the algorithm is quite straightforward and the step by step implementation procedures are outlined in SubSection III-F. In the following discussion, equations that need to be implemented for the algorithm are placed inside boxes.

For mathematical tractability, this section discusses the technique of detecting only the rth sinusoid in the signal model in (1). The detection procedure for the other sinusoids shall be the same as for the rth sinusoid. Define the DFT of the tapered measurement data as

$$Y_k(f_m) = \sqrt{\frac{T_s}{NU_k}} \left(\sum_{n=0}^{N-1} y(n)w_k(n)e^{-j2\pi f_m nT_s} \right), \quad (4)$$

where, $f_m = \frac{mf_s}{N^{(0)}}$ for $0 \le m \le \frac{N^{(0)}}{2}$ are discrete frequency bins at which the DFT is evaluated, and $N^{(0)} \ge N$ is zero-padded length [27]. The tapers (windows) $w_k(n)$ for $k = 0, 1, ..., K-1$, where K is the number of tapers and $K \ge 2$, are restricted to orthogonal windows, that is,

$$\sum_{n=0}^{N-1} w_k(n)w_{k'}(n) = \begin{cases} NU_k, & \text{if } k' = k \\ 0, & \text{otherwise,} \end{cases} \quad (5)$$

with accompanying scaling term for the kth taper

$$U_k = \frac{1}{N} \sum_{n=0}^{N-1} w_k^2(n). \quad (6)$$

Let, $f_{r'} = \frac{r'f_s}{N^{(0)}}$ for $0 < r' < \frac{N^{(0)}}{2}$ be the frequency bin nearest to the FO frequency f_r. Define frequency error as

$$f_r^{\text{err}} = f_{r'} - f_r, \quad (7)$$

where $-\frac{f_s}{2N^{(0)}} \le f_r^{\text{err}} \le \frac{f_s}{2N^{(0)}}$. It is reasonable to assume that f_r^{err} is uniformly distributed over $[-\frac{f_s}{2N^{(0)}}, \frac{f_s}{2N^{(0)}}]$ with $\mathbb{E}\{f_r^{\text{err}}\} = 0$, where $\mathbb{E}\{\cdot\}$ denotes expectation of the underlying quantity with respect to an appropriate statistical distribution [26]. Also, $f_r^{\text{err}} \approx 0$ when $N^{(0)}$ is large. At $f_m = f_{r'}$, according to [25], [28] the following complex-valued regression model can be written from (1) and (4) for the rth FO,

$$Y_k(f_{r'}) = C_r W_k(f_r^{\text{err}}) + E_k(f_{r'}), \ k = 0, 1, .., K-1 \quad (8)$$

where

$$E_k(f_{r'}) = \sqrt{\frac{T_s}{NU_k}} \left(\sum_{n=0}^{N-1} \eta(n)w_k(n)e^{-j2\pi f_{r'}nT_s} \right), \quad (9)$$

and

$$C_r = \frac{1}{2} A_r e^{j\phi_r}. \quad (10)$$

This is where the DFT windowed indicator function evaluated at f_r^{err} is

$$W_k(f_r^{\text{err}}) = \sqrt{\frac{T_s}{NU_k}} \left(\sum_{n=0}^{N-1} w_k(n)I_r(n)e^{-j2\pi f_r^{\text{err}}nT_s} \right), \quad (11)$$

where the tapers have good protection against leakage by concentrating most of the energy within bandwidth $[-B, B]$ Hz. For online detection of FO in synchrophasor measurements the value of $n_e(r)$, $n_s(r)$, and f_r^{err} are typically not known. Therefore, the expected value of zero can be used for f_r^{err} and $I_r(n) = 1 \ \forall \ n$ can be assumed while implementing the detection algorithm for practical applications. Here the symbol "$\forall$" denotes the universal quantifier. However, as will be discussed later, (11) is also useful for analyzing the performance of the detector considering the duration and frequency error of the rth FO.

Based on the regression model (8), the following hypotheses can be tested for detecting whether an FO at f_r is present or not in the analysis window $\mathbf{y}$

$$H_0 : C_r = 0$$
$$H_1 : C_r \ne 0. \quad (12)$$

The null hypothesis H_0 is that the measurements $\mathbf{y}$ do not contain an FO at f_r, and the alternative hypothesis H_1 is that the measurements $\mathbf{y}$ do contain an FO at f_r. A statistical test can then be performed to accept or reject the null hypothesis H_0, and following subsections describe the test and the statistical analyses for the test.

A. Test Statistic and Distribution

For developing a test statistic (see [26], [29]) from the regression model in (8) it is necessary to meet requirements of complex-valued regression theory [28], [30]. In [23], Khan et al. showed the ambient noise $\eta(n)$ is approximately Gaussian for a wide variety of power system conditions. Since $\eta(n)$ is a real-valued zero-mean approximately Gaussian process, in steady-state operating condition of the power system $E_k(f_{r'})$ must follow a complex Gaussian distribution with zero mean [28], [31]. When the ambient noise in the detection window is approximately Wide-Sense-Stationary (WSS), all $E_k(f_{r'})$, $k = 0, 1, .., K-1$, must have the same variance which will be governed solely by the ambient noise power at frequency $f_{r'}$. Also, since the tapers $w_k(n)$ for $k = 0, 1, ..., K-1$ are orthogonal, $E_k(f_{r'})$ terms are approximately pairwise uncorrelated when the ambient noise spectrum is slowly varying in the interval $[f_{r'} - B, f_{r'} + B]$ Hz [28]. In addition, according to [31] real and imaginary parts of $E_k(f_{r'})$ are independent and they have the same variance when $f_{r'}$ is not very close to 0 or $\frac{f_s}{2}$. As requirements are met, following the results of complex-valued regression theory in [30] and harmonic analyses in [25]

and [28], a test statistic can be formed as

$$T(\mathbf{y}, f_{r'}) = \frac{(K-1)\left|\hat{C}_r\right|^2 \sum_{k=0}^{K-1}|W_k(f_r^{\mathrm{err}})|^2}{\sum_{k=0}^{K-1}\left|Y_k(f_{r'}) - \hat{C}_r W_k(f_r^{\mathrm{err}})\right|^2}, \quad (13)$$

where

$$\hat{C}_r = \frac{\sum_{k=0}^{K-1} W_k^*(f_r^{\mathrm{err}}) Y_k(f_{r'})}{\sum_{k=0}^{K-1}\left|W_k(f_r^{\mathrm{err}})\right|^2}, \quad (14)$$

$f_r^{\mathrm{err}} \approx 0$, and the symbol "*" denotes complex conjugation of the underlying quantity. Although the above expressions (13) and (14) are evaluated at $f_r^{\mathrm{err}} \approx 0$ for practical implementation of the detector, if needed, they can be estimated for different values of $f_r^{\mathrm{err}} \in \left[-\frac{f_s}{2N^{(0)}}, \frac{f_s}{2N^{(0)}}\right]$ to investigate how the performance of the detector varies for different frequency errors. The estimate $\hat{C}_r$ in (14) is a minimum variance linear unbiased estimate of C_r [30]. It follows from [30] that, under the null hypothesis H_0, $T(\mathbf{y}, f_{r'}) \sim F_{2,2K-2}$ (i.e., the test statistic is statistically distributed as central F-distribution with numerator and denominator degrees of freedom 2 and $2K-2$, respectively), where "$\sim$" denotes *statistically distributed as*. And, under H_1, $T(\mathbf{y}, f_{r'}) \sim F'_{2,2K-2}(\lambda)$ (noncentral F-distribution with numerator and denominator degrees of freedom 2 and $2K-2$, respectively) with the noncentrality parameter $\lambda = K \times \mathrm{SNR}_o(r)$. The output signal-to-noise ratio [27]

$$\mathrm{SNR}_o(r) = N_s(r) \times \mathrm{ASCG}_{[n_s(r), n_e(r)]}(f_r^{\mathrm{err}}) \times \mathrm{SNR}(r), \quad (15)$$

where $\mathrm{SNR}(r) = \frac{A_r^2 T_s/2}{S_{\eta\eta}(f_{r'})}$ is rth sinusoid power to ambient noise power spectrum at $f_{r'}$ ratio, and average squared coherent gain (ASCG) of tapers is defined as

$$\mathrm{ASCG}_{[n_s(r), n_e(r)]}(f_r^{\mathrm{err}}) = \frac{1}{KT_s N_s(r)} \sum_{k=0}^{K-1}\left|W_k(f_r^{\mathrm{err}})\right|^2, \quad (16)$$

where $N_s(r) = n_e(r) - n_s(r) + 1$ is the duration of the rth FO in the detection window. The value of $N_s(r)$ is non-zero if the rth FO is present in the detection window $\mathbf{y}$. Otherwise, $N_s(r) = 0$, which makes the $\mathrm{SNR}_o(r)$ to be zero for the rth FO. Following Cauchy inequality defined in [28] and using the fact that $0 \le N_s(r) \le N$, it can be shown that the ASCG is bounded by the limit $[0, 1]$. For a set of K orthogonal tapers described in SubSection III-C, the ASCG takes on a value within $[0, 1]$ close to its maximum when $N_s(r) = N$ provided that $N_s(r)$ is not insignificant compared to N, and zero when $N_s(r) = 0$. Also, ASCG remains fairly constant when f_r^{err} is close to zero. It is important to emphasize that the test statistic $T(\mathbf{y}, f_{r'})$ in (13) does not require any prior knowledge of the system, and its calculation requires only the PMU measurements, when windows are already chosen.

With the test statistic established in (13), the hypothesis test in (12) can be performed by rejecting the null hypothesis when $T(\mathbf{y}, f_{r'})$ exceeds some threshold γ such that $\gamma \ge 0$.

The $\mathrm{SNR}_o(r)$ in (15) provides a wealth of information about the test. It shows that the probability of detecting an FO increases with the increase in $\mathrm{SNR}(r)$, ASCG, and duration of the FO $N_s(r)$ in the detection window $\mathbf{y}$. These results are intuitive as one would expect that high signal-to-noise ratio (SNR), long duration sinusoids should be associated with high probability of detection. When there is no FO present, SNR_o becomes zero as $N_s(r) = 0$, and correspondingly the test statistic will follow the $F_{2,2K-2}$ distribution under the null hypothesis. The following subsection discusses more about the performance of this detector along with how to choose the detection threshold.

B. Detection Threshold and Detector Performance

As is common practice, the detection threshold is set to achieve a desired probability of false alarm, P_{FA} [2], [29]. The performance of the detector can be expressed by P_{FA} and P_D [2], [29]. A false alarm occurs if the test statistic $T(\mathbf{y}, f_{r'})$ exceeds the threshold γ even though there is no FO at f_r present in the detection segment $\mathbf{y}$. Following the $F_{2,2K-2}$ distribution under the null hypothesis H_0 and cumulative distribution function (CDF) definition of central F-distribution in [29], the P_{FA} can be expressed as

$$P_{FA} = P(T(\mathbf{y}, f_{r'}) > \gamma | H0) = \left(\frac{K-1}{K-1+\gamma}\right)^{K-1}, \quad (17)$$

here the notation $P(A|B)$ denotes the probability of A given B is true. Note that when $\gamma = 0$, $P_{FA} = 1$, and this confirms non-negative support of the F-distribution, and hence, $T(\mathbf{y}, f_{r'})$ and γ must be greater than or equal to zero. The threshold γ is then expressed in terms of P_{FA} by rearranging (17) as

$$\gamma = (K-1) \times \left(e^{\frac{\ln(P_{FA})}{1-K}} - 1\right), \quad (18)$$

where $\ln(\cdot)$ is the natural logarithm. Using this expression, the threshold γ can be determined for a particular setting of K and P_{FA} when detecting an FO at f_r. In practice a number of frequency bins (say N_F) within $[f_{\min}, f_{\max}]$ Hz are investigated for detecting FOs, and correspondingly, the threshold in (18) needs to be modified to account for all the frequency bins. When there is no zero-padding, the test statistic in (13) are independent from one frequency bin to another provided that B is smaller than separation between two consecutive frequency bins in (4). If zero-padding is used or B is large, the test statistics remain no longer independent from one frequency bin to another for all frequency bins, and therefore, an exact expression for P_{FA} cannot be obtained. Following similar reasoning in [2], and using a general version of the Bonferroni inequality in [26], the threshold γ can be modified to account for N_F frequency bins such that the P_{FA} will not exceed $P_{FA}^{\max}$ as

$$\gamma' = (K-1) \times \left(e^{\frac{1}{1-K} \ln\left(\frac{P_{FA}^{\max}}{N_F}\right)} - 1\right). \quad (19)$$

Notice that the expression of P_{FA} or γ' is independent of the measurements $\mathbf{y}$, and therefore, once the γ' is set the detector performs with a constant false alarm rate [29].

When an FO of frequency f_r is present in the detection segment $\mathbf{y}$, the detector can detect the FO with probability

$$P_D = P(T(\mathbf{y}, f_{r'}) > \gamma | H1) = 1 - \left(\frac{\gamma}{\gamma + K - 1} \right)$$
$$\times \left[\exp\left\{ -\frac{1}{2} \times K \times \mathrm{SNR}_o \times \left(\frac{K-1}{\gamma + K - 1} \right) \right\} \right] \sum_{i=0}^{K-2} \mathcal{T}_i \tag{20}$$

where $\mathcal{T}_i$ for $i = 1, 2, ... K - 2$ are recurrence functions defined as

$$\mathcal{T}_{-1} = 0, \ \ \mathcal{T}_0 = 1,$$
$$\mathcal{T}_i = \frac{1}{i} \left(\frac{K-1}{\gamma + K - 1} \right) \left[\left(2i - 1 + \frac{K \times \mathrm{SNR}_o \times \gamma}{2(\gamma + K - 1)} \right) \mathcal{T}_{i-1} \right.$$
$$\left. - (i - 1) \left(\frac{K-1}{\gamma + K - 1} \right) \mathcal{T}_{i-2} \right]. \tag{21}$$

The above expressions (20) and (21) follow from the CDF of the non-central F-distribution defined in [32] following simplification using the fact that $2K - 2$ is an even integer [33]. Although the expressions look quite complicated, the end result is intuitive. For a particular setting of K and P_{FA}, P_D increases with the increase in SNR_o, and as described previously the SNR_o increases with the increase in power or duration of FO in the detection segment. The expression of P_D shows a great deal of information about the detector performance, such as how its FO detection capability varies with SNR level, detection window length, and the duration of the FO in the detection window. In Section IV, how the probability of detection P_D varies with different $\mathrm{SNR}(r)$ levels will be shown along with experimental results from simulation studies.

C. Choice of Tapers and K

As mentioned previously, the tapers need to be orthogonal for $E_k(f_{r'})$, $k = 0, 1, .., K - 1$, to be pairwise uncorrelated, and optimally concentrated in frequency $[-B, B]$ Hz to minimize bias in spectral estimates. The optimal tapers that satisfy these requirements are Discrete Prolate Spheroidal or Slepian Sequences (DPSS) [34]. Briefly, the DPSS sequences are derived from following time-frequency concentration eigenvalue maximizing problem

$$\lambda(N, B) = \frac{\int_{-B}^{B} |W(f)|^2 df}{\int_{-\frac{f_s}{2}}^{\frac{f_s}{2}} |W(f)|^2 df}, \tag{22}$$

where $W(f)$ is the Discrete Time Fourier Transform (DTFT) of a window $w(n)$, and $\lambda(N, B) : 0 < \lambda < 1$ represents the fraction of the window energy for a time-half bandwidth product NB. For a particular NB, the closer λ gets to one, the more energy concentration happens within the band $[-B, B]$ for the corresponding eigenvector, and hence less leakage (or bias) is obtained. These eigenvectors are the DPSS sequences, and they are orthonormal, i.e., $U_k = \frac{1}{N}$ for all k [28], [34]. The eigenvalues corresponding to K DPSS tapers will be very close to one

if the value of K is chosen to be less than the Shannon number $2NBT_s$. Thus, a value of K close to $2NBT_s - 1$ is chosen typically for many multitaper spectral estimation applications [28]. The calculation of DPSS sequence directly from their definition is difficult due to instability of the calculations, and therefore, they are typically approximated with different numerical techniques. A few methods of calculating DPSS tapers can be found in [28]. Detailed discussion on the multitaper estimation, and DPSS sequences and their generation are beyond the scope of this paper. Interested readers are referred to [25], [28], [34] for more details.

A much simpler set of sine orthogonal tapers for multitaper spectral analysis was suggested by Riedel *et al.* in [35]. The kth member of the sine tapers is given by

$$\boxed{w_k(n) = \sqrt{\frac{2}{N+1}} \sin\left(\frac{(k+1)\pi(n+1)}{N+1} \right).} \tag{23}$$

These are just harmonically related sine windows. The sine tapers achieve much smaller local bias (bias introduced due to the smoothing by the main lobe of a window [36]) compared to that of the DPSS sequences at the expense of sidelobe suppression [35], [36]. For many applications the sinusoidal tapers works as well as the DPSS sequences, and use of K sine tapers provides a multitaper estimator with spectral window concentrated approximately in the interval $\left[-\frac{f_s(K+1)}{2(N+1)}, \frac{f_s(K+1)}{2(N+1)} \right]$ Hz [36]. The sine tapers are normalized so that they become orthonormal.

For detecting FOs in power system, once the type of tapers is chosen, the number of tapers K can be determined by specifying half resolution bandwidth B for a detection segment of length N such that $NBT_s \geq 1.5$. For a specified B the detector will have a spectral resolution bandwidth of $2B$ meaning it will not be able to distinguish two FOs when they are spaced less than B Hz. Therefore, a value of B can be chosen as large as the frequency resolution constraint of the application at hand. Once the half-bandwidth B is specified, a number close to $\lfloor 2NBT_s \rfloor$ (here $\lfloor . \rfloor$ represents the floor function) can be chosen for K. Note that the tapers are computed and stored once before the detector is employed. The stored tapers are then used by the detection algorithm for detecting periodic FOs in power system.

D. Multiple Detection Segment

When the duration of the rth FO in the detection window $\mathbf{y}$ of length N increases, the terms $N_s(r)$ and ASCG in (15) increase. This increases the detection probability P_D in (20). In addition, the detection probability also increases with the increase in the number of tapers K. But, the value of K is limited by the time-half bandwidth product NB for tapers with good leakage properties. Therefore, K cannot be increased without sacrificing the frequency resolution of the detector for a small detection window. However, for a strong FO the $\mathrm{SNR}(r)$ is high. As a result, a small segment can be used for detecting strong FOs without significantly decreasing the detector performance. This would be useful for early detecting strong FOs. Larger detection windows can be used for reliably detecting small but persistent

FOs in the measurements. These results are similar to that of the periodogram based FO detection algorithm in [2].

E. Refining Detected FOs

Ideally, there should be a single detection at frequency f_r corresponding to the rth FO. Because of leakage and zero-padding more than one FO may be detected near f_r. For a finite length detection window, if non-integer number of periods of the rth FO is captured in the measurements $\mathbf{y}$, the frequency content of the FO will leak into nearby frequency bins of $f_{r'}$ in the DFT estimate of (4). This will result in multiple detections corresponding to only the rth FO. Furthermore, although zero-padding improves the frequency estimates of detected FOs, it does not improve the frequency resolution provided by the orthogonal tapers (and hence the detector), as the frequency resolution depends on the length of the measurements N, not on the zero-padded length $N^{(0)}$ [37]. As a result, there will be multiple detection corresponding to a single FO at frequencies around the frequency bin nearest to the true FO frequency. As frequency resolution of the detector is limited by the half-bandwidth B, the detected FOs within $[f_{r'} - B, f_{r'} + B]$ Hz need to be refined. This can be achieved by discarding all detected FOs within $[f_{r'} - B, f_{r'} + B]$ Hz except the FO at $f_{r'}$. For a group of detected FOs within $[f_{r'} - B, f_{r'} + B]$ Hz, the value of $\hat{C}_r$ will be maximum at $f_{r'}$.

In addition, there will be duplicate detection corresponding to the rth FO when multiple detection segments technique is employed. The duplicate frequencies can be refined by discarding detected frequencies in small detection window that fall within resolution bandwidth of detected frequencies of longer detection window. This gives more preference of detections in longer detection windows than shorter windows (similar to the refining method in [2]).

F. Procedure for Detecting FOs

The flowchart in Fig. 1 shows the overall process of the detection algorithm for detecting FOs in power systems. Relevant sections/subsections to implement the algorithm are listed to the left/right of each block. Design of the detector (steps I–IV) are performed once before the detector is employed. After that, the detection processes (steps V–IX) are performed in an online environment.

IV. EXPERIMENTAL RESULTS

The statistical performance of the detector described in the previous section was verified using multiple trials of simulated data in the following subsection. The detector was then applied to field measured PMU data collected from the Western Electricity Coordinating Council (WECC) system. In each case, a relative frequency signal was derived from two voltage angles by taking the derivative of their difference. In the relative frequency signal, the speed-governor effects are removed and such a signal enables useful modal and spectral analyses of the power system [2], [38].
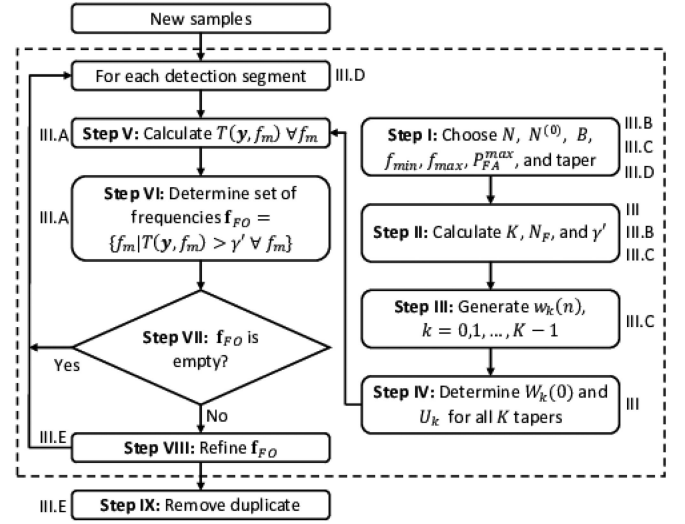

Fig. 1. Flow chart describing the detection algorithm. Relevant sections/subsections are listed to the left/right of each block.

A. Results From Simulated Data

In this subsection the performance of the detector is discussed based on simulation studies and compared to theoretical values. Using the MinniWECC model [39] 10,000 trials of 10 min. long relative frequency signals were generated at 120 samples per sec. The higher sampling rate was used to reflect the upper end capabilities of PMUs. Other sampling rates can be used as long as the frequency content of interest is less than the folding frequency. The MinniWECC is a reduced order dynamic model that is geographically consistent with the WECC system and it represents overall inter-area modal properties of the WECC system. More about the model can be found in [39] and the references therein. The model enables some percent of constant real and reactive power loads to vary over time. The random load variations provide small excitations to the dynamics of the system which results in ambient noise at the system output in steady-state conditions [23]. The model also enables adding a square wave at a generator bus to reflect the generator entering a stable limit cycle [2]. Fundamental and its harmonic components within the square wave are considered FOs in the system measurements, and they are characterized by their corresponding amplitudes and frequencies. In this study the frequency of the fundamental component of the square wave was set to 0.3719 Hz, right at one of the dominant modes of the system to consider the most extreme case. The amplitude of the square wave was varied for achieving specific $\mathrm{SNR}(r)$ levels for the 0.3719 Hz FO in the system outputs.

The detector was applied to simulated relative frequency signals with settings $N = 7.2 \times 10^4$ (10 min.), $N^{(0)} = 5N$, $B = 7.5 \times 10^{-3}$ Hz, $f_{\min} = 0.1$ Hz, $f_{\max} = 1.5$ Hz, and $K = 9$ DPSS tapers. The detection window of length 10 min. was used to enabling higher number of tapers ($K = 9$) to be used for the detection algorithm as the detectors detection probability in (20) increases with increase in number of tapers K for a particular setting of $P_{FA}^{\max}$ while achieving a high frequency resolution of
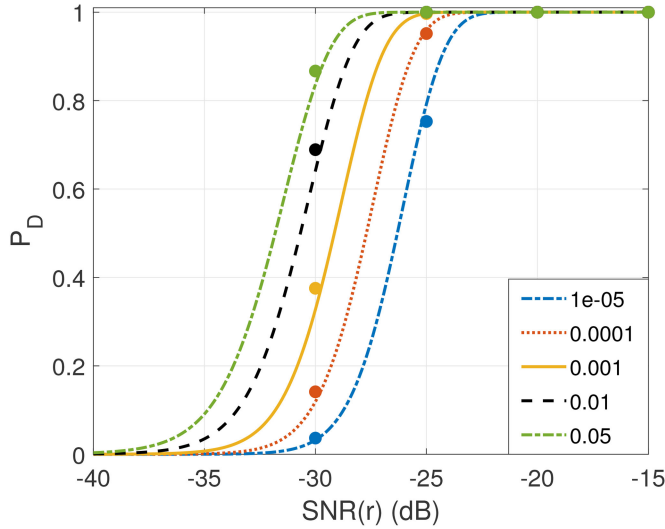
Fig. 2. Theoretical P_D at different $\mathrm{SNR}(r)$ levels (solid curves) for various $P_{\mathrm{FA}}^{\max}$ values. Estimated P_D (dots) from 10, 000 simulations are also shown.
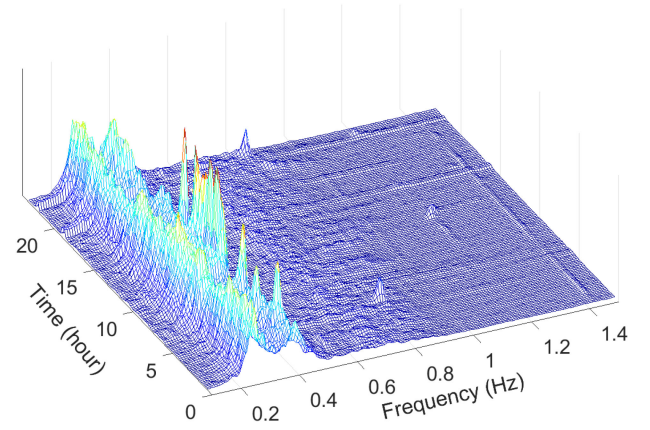

Fig. 3. Waterfall plot of Welch PSD estimates from a 24 hour long relative frequency signal derived from two voltage angles measured at two distinct locations in the WECC system.
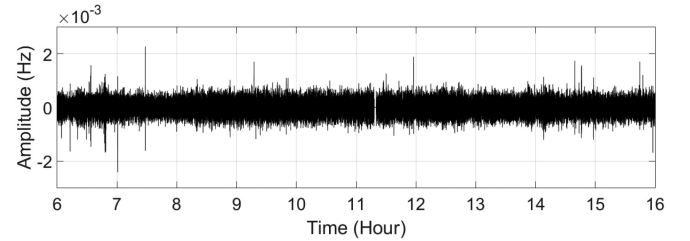

Fig. 4. Time domain plot of the signal used to generate Fig. 3. Only 6–16 hours data is shown.

$B = 7.5 \times 10^{-3}$ Hz. This provides a close approximation of the threshold in (19) for a particular setting of $P_{FA}^{\max}$ as the number of uncorrelated frequency bins in (4) within $[f_{\min}, f_{\max}]$ increases with the increase in frequency resolution. This further provides a close approximation of the experimental probability of false alarm of the detector towards true value of $P_{FA}^{\max}$. For all trials the 0.3719 Hz FO was always present in the detection window. From the detection results, the P_D was estimated and Fig. 2 shows the estimates (dots) for different $P_{\mathrm{FA}}^{\max}$ values at various $\mathrm{SNR}(r)$ levels along with their corresponding theoretical values (curves) from (20). The threshold specified in (19) was used for the detection algorithm. The simulated results in the figure suggests that the detector is working as expected. Similar results were observed when sine tapers were used instead of the DPSS tapers and different detection parameter settings were used.

In addition to the P_D, the probability of false alarm was determined experimentally by applying the detection algorithm to simulated datasets where there was no FO present. The same parameters setting that was used for estimating the P_D was also used for determining the experimental probability of false alarm. When, the $P_{\mathrm{FA}}^{\max}$ was set to 10^{-3} and 10^{-4} the experimental false alarm rate was observed to be 1.3×10^{-3} and 1.0×10^{-4}, respectively, from 10,000 trials. The results show that the detection algorithm performs as expected.

B. Results From Measured Data

To illustrate the practical application of this forced oscillation detector, it was applied to WECC datasets with both large and small FOs. The PMU data analyzed in this subsection were captured at 30 samples per sec. The relative frequency signals were first filtered with a finite impulse response equiripple filter having passband and stopband frequencies 1.5 and 2.5 Hz, and ripples 0.02 and 50 dB, respectively. The signals were then downsampled to five samples per sec. and highpass filtered with

a single-pole single-zero 0.015 Hz cutoff frequency infinite impulse response filter. The highpass filter attenuates very low frequency trends or speed-governor effects in the signal. This preprocessing was used to focusing FO detection on the frequency range of the inter-area modes [40].

The first set of data is a 24-hour long relative frequency signal derived from two voltage angles measured at two geographically distinct locations in the WECC system in January 2009. The two locations were chosen so as to achieve strong visibility of two typical dominant electromechanical modes (North/South-A and North/South-B) in the relative frequency signal. The signal was preprocessed and Fig. 3 shows Welch averaged waterfall plot of spectral estimates of the preprocessed signal [38]. A 30 min. long measurement window with a 80% overlapped two min. long squared Von Hann window were used to obtain the Welch PSD estimates. A new estimate was obtained every 10 min. using most recent 30 min. long measurements. In the plot two dominant modes of the WECC system near 0.25 and 0.4 Hz are clearly visible along with an intermittent FO very close to the 0.4 Hz mode. During 9.5–11.5 hours the FO is consistently present in the measurements with varying amplitudes. The time domain signal in Fig. 4 shows the FO is buried in the ambient noise of the system as its amplitude is very small. Notice that there is a 110 sec. long missing data window in the signal at around 11.32-hour.

The detection algorithm described in Section III was applied to the relative frequency signal and Fig. 5 shows the detection
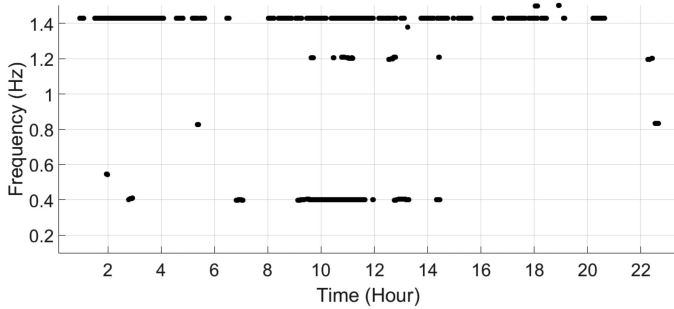
Fig. 5.   Output of the detection algorithm when applied to the signal used to generate Fig. 3.
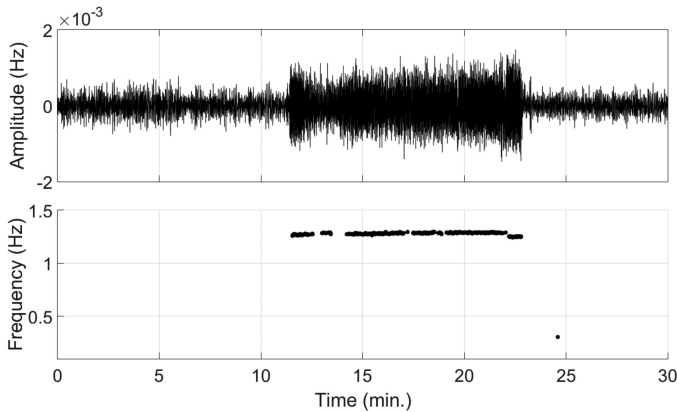

Fig. 6.   Detection algorithm output (bottom) when applied to the time-domain signal (top) containing a strong FO.

results. The detection parameters were set as follows: $N = 3 \times 10^3$ (10 min.), $N^{(0)} = 3 \times 10^4$, $B = 0.05$ Hz, $f_{\min} = 0.1$ Hz, $f_{\max} = 1.5$ Hz, $P_{\mathrm{FA}}^{\max} = 10^{-4}$, and $K = 60$ DPSS tapers. The detection algorithm was applied every minute to most recent 10 min. measurements to generate the figure. The FO near 0.4 Hz is well captured by the detection algorithm. When present very low amplitude third harmonic of the FO near 1.2 Hz is also captured by the detector. It also detected a consistent FO near 1.4 Hz which is barely visible in the waterfall plot in Fig. 3. There is an occasional FO near 0.8 Hz which was also detected by the detector. Similar results were observed when the detector was applied to this dataset with sine tapers instead of DPSS.

Another set of data was captured when a small power plant in the WECC system was generating a large FO near 1.28 Hz in February 2010. Once again, a relative frequency signal was derived from two voltage angles. The signal was preprocessed and the detector was applied to the preprocessed signal with following setup: $N = 50$ (10 sec.), $N^{(0)} = 5 \times 10^3$, $B = 0.25$ Hz, $f_{\min} = 0.1$ Hz, $f_{\max} = 1.5$ Hz, $P_{FA}^{\max} = 10^{-4}$, and $K = 6$ DPSS tapers. Fig. 6 shows the time domain signal and the detector output. The FO starts and ends at approximately 11.4 and 22.8 min., respectively, and is well captured by the detector while having a very low false alarm rate. This is significant from operators perspective as it allows early detection of strong FOs. Similar results were also observed when the detector was applied to this dataset with sine tapers instead of DPSS. Also, the algorithm was tested using a few other datasets containing different FO amplitudes, frequencies, and durations, and similar positive test results were observed.

V. CONCLUSION

An algorithm based on Thomson's multitaper spectral estimation and harmonic analysis technique was proposed for the detection of periodic FOs in power system. The algorithm compares a test statistic derived from only synchrophasor measurements to a threshold and for setting the threshold no prior system knowledge is required. Based on the test statistic's distribution, a general expression for the threshold relating probability of false alarm of the detector was provided. An expression of probability of detection of the FO detection algorithm was also provided. Simulation studies were carried out for testing the algorithm for ensuring its proper functionalities. The detector was then applied to two field measured datasets. The detector successfully detected the FO very close to the 0.4 Hz dominant electromechanical mode of the WECC system in the first dataset using a 10 min. window. It also detected a few other very small intermittent FOs in the measurements. The strong FO in the second dataset was well captured by the detector with a very small (10 sec.) window. Both of these results are significant as FOs near dominant modes of the system are harder to detect, and strong FOs need to be detected as early as possible. The results suggest that the proposed algorithm is applicable to detecting periodic FOs in power system in near real-time.

ACKNOWLEDGMENT

REFERENCES

[1] L. Vanfretti *et al.*, "Application of ambient analysis techniques for the estimation of electromechanical oscillations from measured PMU data in four different power systems," *Eur. Trans. Elect. Power*, vol. 21, no. 4, pp. 1640–1656, 2010.

[2] J. Follum and J. W. Pierre, "Detection of periodic forced oscillations in power systems," *IEEE Trans. Power Syst.*, vol. 31, no. 3, pp. 2423–2433, May 2016.

[3] M. Ghorbaniparvar, "Survey on forced oscillations in power system," *J. Modern Power Syst. Clean Energy*, vol. 5, no. 5, pp. 671–682, 2017.

[4] W. Xuanyin, L. Xiaoxiao, and L. Fushang, "Analysis on oscillation in electro-hydraulic regulating system of steam turbine and fault diagnosis based on PSOBP," *Expert Syst. Appl.*, vol. 37, no. 5, pp. 3887–3892, 2010.

[5] J. E. Van Ness, "Response of large power systems to cyclic load variations," *IEEE Trans. Power App. Syst.*, vol. PAS-85, no. 7, pp. 723–727, Jul. 1966.

[6] M. Magdy and F. Coowar, "Frequency domain analysis of power system forced oscillations," *IEE Proc. C, Gener., Transmiss. Distrib.*, vol. 137, no. 4, pp. 261–268, Jul. 1990.

[7] P. B. Reddy and I. A. Hiskens, "Limit-Induced stable limit cycles in power systems," in *Proc. IEEE Russia Power Tech*, 2005, pp. 1–5.

[8] A. Silverstein, "Diagnosing equipment health and misoperations with PMU Data," North Amer. SynchroPhasor Initiative, Tech. Rep. NASPI-2015-TR-009, May 2015. [Online]. Available: https://www.naspi.org/sites/default/files/reference_documents/14.pdf?fileID=1530

[9] R. B. Myers and D. J. Trudnowski, "Effects of forced oscillations on spectral-based mode-shape estimation," in *Proc. IEEE Power Energy Soc. Gen. Meeting*, 2013, pp. 1–6.

[10] Y.-H. Wan, "Synchronized phasor data for analyzing wind power plant dynamic behavior and model validation," Nat. Renewable Energy Lab., Golden, CO, USA, Tech. Rep. NREL/TP-5500-57342, Jan. 2013. [Online]. Available: https://www.nrel.gov/docs/fy13osti/57342.pdf

[11] C. D. Vournas, N. Krassas, and B. C. Papadias, "Analysis of forced oscillations in a multimachine power system," in *Proc. Int. Conf. Control*, Mar. 1991, pp. 443–448.

[12] S. A. N. Sarmadi and V. Venkatasubramanian, "Inter-Area resonance in power systems from forced oscillations," *IEEE Trans. Power Syst.*, vol. 31, no. 1, pp. 378–386, Jan. 2016.

[13] J. W. Pierre, D. J. Trudnowski, and M. K. Donnelly, "Initial results in electromechanical mode identification from ambient data," *IEEE Trans. Power Syst.*, vol. 12, no. 3, pp. 1245–1251, Aug. 1997.

[14] D. J. Trudnowski, J. W. Pierre, N. Zhou, J. F. Hauer, and M. Parashar, "Performance of three mode-meter block-processing algorithms for automated dynamic stability assessment," *IEEE Trans. Power Syst.*, vol. 23, no. 2, pp. 680–690, May 2008.

[15] J. Follum, J. W. Pierre, and R. Martin, "Simultaneous estimation of electromechanical modes and forced oscillations," *IEEE Trans. Power Syst.*, vol. 32, no. 5, pp. 3958–3967, Sep. 2017.

[16] J. D. Follum, "Electromechanical mode estimation in the presence of forced oscillations," Ph.D. dissertation, Dept. Elect. Comput. Eng., Univ. Wyoming, Laramie, WY, USA, 2014.

[17] N. Zhou, "A coherence method for detecting and analyzing oscillations," in *Proc. IEEE Power Energy Soc. Gen. Meeting*, 2013, pp. 1–5.

[18] N. Zhou and J. Dagle, "Initial results in using a self-coherence method for detecting sustained oscillations," *IEEE Trans. Power Syst.*, vol. 30, no. 1, pp. 522–530, Jan. 2015.

[19] M. Donnelly, D. Trudnowski, J. Colwell, J. Pierre, and L. Dosiek, "RMS-energy filter design for real-time oscillation detection," in *Proc. Power Energy Soc. Gen. Meeting*, Denver, CO, USA, 2015, pp. 1–5.

[20] D. Kosterev *et al.*, "Implementation and operating experiences with oscillation detection application at Bonneville Power Administration," in *Proc. CIGRE Grid Future*, Philadelphia, PA, USA, 2016.

[21] J. Follum and F. Tuffner, "A multi-channel method for detecting periodic forced oscillations in power system," in *Proc. IEEE Power Energy Soc. Gen. Meeting*, Jul. 2016, pp. 1–5.

[22] J. D. Follum, "Detection of forced oscillations in power system with multichannel methods," Pacific Northwest Nat. Lab., Richland, WA, USA, Tech. Rep. PNNL-24681, 2015. [Online]. Available: http://www.pnnl.gov, Accessed on: Apr. 2017.

[23] M. A. Khan, J. W. Pierre, D. J. Trudnowski, and S. S. Wulff, "An initial study of ambient noise in synchrophasor measurements," in *Proc. North Amer. Power Symp.*, Denver, CO, USA, Sep. 2016, pp. 1–6.

[24] J. Follum, F. Tuffner, and U. Agrawal, "Application of a new nonparametric estimator of ambient power system spectra for measurements containing forced oscillations," in *Proc. IEEE Power Energy Soc. Gen. Meeting*, Jul. 2017, pp. 1–5.

[25] D. J. Thomson, "Spectrum estimation and harmonic analysis," *Proc. IEEE*, vol. 70, no. 9, pp. 1055–1096, Sep. 1982.

[26] G. Casella and R. L. Berger, *Statistical Inference*, 2nd ed. Pacific Grove, CA, USA: Brooks/Cole, 2002.

[27] B. Porat, *A Course in Digital Signal Processing*. New York, NY, USA: Wiley, 1997.

[28] D. B. Percival and A. T. Walden, *Spectral Analysis for Physical Applications: Multitaper and Conventional Univariate Techniques*. New York, NY, USA: Cambridge Univ. Press, 1993.

[29] S. M. Kay, *Fundamentals of Statistical Signal Processing, Detection Theory*, vol. II. Englewood Cliffs, NJ, USA: Prentice-Hall, 1998.

[30] K. S. Miller, "Complex Linear Least Squares," *SIAM Rev.*, vol. 15, no. 4, pp. 706–726, 1973.

[31] D. R. Brillinger, *Time Series: Data Analysis and Theory*. Philadelphia, PA, USA: SIAM, 2001.

[32] N. Johnson, S. Kotz, and N. Balakrishnan, *Continuous Univariate Distributions*, vol. 2. Hoboken, NJ, USA: Wiley, 1995.

[33] M. Sibuya, "On the noncentral beta distribution function," *unpublished*.

[34] D. Slepian, "Prolate Spheroidal Wave Functions, Fourier Analysis, and Uncertainty—V: The Discrete Case," *The Bell Sys. Tech. J.*, vol. 57, no. 5, pp. 1371–1430, 1978.

[35] K. S. Riedel and A. Sidorenko, "Minimum bias multiple taper spectral estimation," *IEEE Trans. Signal Process.*, vol. 43, no. 1, pp. 188–195, Jan. 1995.

[36] E. J. McCoy, A. T. Walden, and D. B. Percival, "Multitaper spectral estimation of power law processes," *IEEE Trans. Signal Process.*, vol. 46, no. 3, pp. 655–668, Mar. 1998.

[37] J. G. Proakis, *Digital Signal Processing: Principles, Algorithms, and Application*, 4th ed. London, U.K.: Pearson, 2007.

[38] D. Trudnowski and T. Ferryman, "Modal baseline analysis of the WECC system for the 2008/9 operating season," Pacific Northwest National Laboratory, Richland, WA, USA, Sep. 2010.

[39] D. Trudnowski and J. Undrill, "The minniWECC system model," Bonneville Power Administration, Portland, OR, USA, 2008.

[40] J. W. Pierre *et al.*, "Overview of system identification for power systems from measured responses," *IFAC Proc. Vol.*, vol. 45, no. 16, pp. 989–1000, Jul. 2012.

Md. Arif Khan (S'15–M'18) received the B.S. degree in electronics and communication engineering (ECE) from the Khulna University of Engineering and Technology (KUET), Khulna, Bangladesh, in 2010, and the M.S. and Ph.D. degrees in electrical engineering from the University of Wyoming (UW), Laramie, WY, USA, in 2014 and 2018, respectively.

From 2010 to 2012, he was a Lecturer with the Department of ECE, KUET. From 2012 to 2014, he was with the Wyoming Image and Signal Processing Research Laboratory, where he worked on an Automatic Control of Light Weight Unmanned Aerial Vehicle Project funded by the NASA Ames Research Center. From 2014 to 2018, he was a Research Fellow with the UW. He is currently a Research Engineer with Schweitzer Engineering Laboratories, Inc., Pullman, WA, USA. His research activities are primarily focused on signal and image processing, statistical signal processing, power system stability, and machine learning.

Dr. Khan was the recipient of the University Gold Medal in 2010, UW Engineering Excellence Fellowship from 2014 to 2018, and the President's Award in Rocky Mountain Bioengineering Symposium, Denver, CO, USA, 2014. He is a member of Tau Beta Pi and Golden Key Honor societies and an associate member of The Institute of Engineers, Dhaka, Bangladesh.

John W. Pierre (S'86–M'86–S'87–SM'99–F'13) received the B.S. degree from Montana State University, Bozeman, MT, USA, in 1986, and the M.S. and Ph.D. degrees from the University of Minnesota, Minneapolis, MN, USA, in 1989 and 1991, respectively, all in electrical engineering.

He was an Electrical Design Engineer with Tektronix, Inc., Beaverton, OR, USA, before joining the University of Minnesota. Since 1992, he has been a Professor with the Department of Electrical and Computer Engineering, University of Wyoming (UW), Laramie, WY, USA. From 2003 to 2004, he was the Interim Department Head. His research interest includes statistical signal processing applied to power systems.

Dr. Pierre is a member of the IEEE Signal Processing, Education, and Power and Energy Societies. He was the recipient of the UW's College of Engineering Graduate Teaching and Research Award in 2005 and the Distinguished Graduate Mentor Award in 2015, which is a university-wide award for outstanding mentorship of graduate students.